Desalination and Water Treatment
www.deswater.com

doi: 10.5004/dwt.2020.26268

204 (2020) 413–428
November

Performance study of activated carbon and silica gel for sorption of CO_2 from a mixture of N_2/CO_2: equilibrium, breakthrough and mass transfer zone

Mohammed K. Al Mesfer[a], Mohd Danish[a], Basem Abdullah Al Alwan[a], Nasser S. Awwad[b,*]

[a]*Chemical Engineering Department, College of Engineering, King Khalid University, 61411 Abha, Saudi Arabia, emails: almesfer@kku.edu.sa (M.K. Al Mesfer), danishmohd111@yahoo.com (M. Danish), beilwan@kku.edu.sa (B.A. Al Alwan)*
[b]*Chemistry Department, College of Science, King Khalid University, 61411 Abha, Saudi Arabia, Tel: +966549323204; email: aawwad@kku.edu.sa (N.S. Awwad)*

Received 19 January 2020; Accepted 7 June 2020

ABSTRACT

Temperature, feed rate, length of mass transfer zone (L_{MTZ}), utilization factor and partial pressure are parameters for fixed bed sorption of carbon dioxide (CO_2) from N_2/CO_2 mixture. The breakthrough time relies strongly on temperature and feed rate. Prolonged breakthrough time and saturation time have been realized for activated carbon (AC). The response curves of AC are vastly steep, signifying the maximal utilization of bed capacity at the breakpoint. In general, the L_{MTZ} increases with a rise in temperature and feed flow rate. The capacity utilization factor reduces with a rise in temperature and feeds flow rate. A utilization factor of 0.919 was determined for AC at a temperature of 298 K. The maximal capacity for CO_2 reduces significantly with an increase in temperature. The maximal capacity of 32.99 g CO_2/kg was obtained at a temperature of 298 K for AC. This capacity improves considerably with CO_2 partial pressure, and AC exhibits higher adsorption capacity when compared to silica gel. The capacity improves considerably with an increase in feed rates, and a maximal capacity of 39.14 g CO_2/kg was found for AC at a feed rate of 8.33×10^{-5} m^3/s. Owing to its high sorption capacity and utilization factor, the AC can be used for the economical separation of CO_2 from the N_2/CO_2 mixture.

Keywords: Sorption; Utilization factor; Breakthrough; Mass transfer zone; Capacity

1. Introduction

Carbon dioxide (CO_2) is the single largest contributor to greenhouse gases, and its increased level in the atmosphere has led to global warming. The combustion of fossil fuels accounts for almost 81% of the energy used for commercial purposes. This process releases 3.0×10^{13} kg of CO_2 every year [1], which contributes more significantly to global warming than other greenhouse gases such as H_2O, CH_4, N_2O and CFCs. The prime environmental concern is regarding the alarming rate at which the CO_2 concentration is rising in the atmosphere [2,3]. The power generation sector between the years 2000 to 2030 will have contributed almost to the total increase in global CO_2 emissions [4]. As much as 45% of the total global CO_2 emission is attributed to thermoelectric and industrial electricity generating plants [5].

The mean global temperature rise by just 2°C can result in far-reaching consequences. Therefore, it is recommended the greenhouse gases be reduced to 50% by the year 2050 [6]. A definite percentage of CO_2 is always associated with the combustion of flue gases that rely on the feedstock. The accessible CO_2-reduction technologies are a potential option for economical cuts in the release of CO_2 in the environment. CO_2 emissions can be reduced by one of the three methods that rely on plant configuration [7]. The treatment of synthesis gas, which is primarily composed of CO and H_2 gases, is performed in the pre-combustion process [8].

* Corresponding author.

Approximately 1.5 times more energy is required in the post-combustion process compared to the pre-combustion method of capturing CO_2 [9]. Primarily, CO_2 and H_2O are the emissions of oxy-fuel combustion [10]. The oxy-fuel process aims to decrease these emissions by 60%–70%. There are primarily four technologies available for CO_2 reduction from the emission of power plants based on fossil fuel.

Chemical and physical absorption is realized by a reaction between CO_2 and a solvent, primarily an amine solution [11]. Amine solutions are utilized for CO_2 absorption from CO_2/air mixture. The capacity of 98.2×10^{-2} mol/mol was reported for diethanolamine [12]. Streams having a CO_2 concentration of more than 50% are normally treated using cryogenic separations [13]. In the case of the CO_2 concentration being more than 20%, the membrane systems are extremely adaptable [14]. The post-combustion CO_2 diminution is mainly a pragmatic process because various suggested technologies can be fit back to the existing plants based on fossil fuel [15–17]. CO_2 reduction by employing adsorption is contemplated as a dry process, and there is no by-product such as water when compared to other conventional processes. Adsorption is considered a well-established technology to capture CO_2 in the post-combustion process [18,19]. The adsorbent preferentially separates CO_2 and, afterward, regenerates to release CO_2 irrespective of the process configuration [18–21].

Fine activated carbons (AC) were employed under sound-assisted fluidization for CO_2 capture, and the experiments reported enhanced adsorption [22]. A fluidized bed column was utilized to analyze the separation of CO_2 from the flue gas feed experimentally [23,24]. An in-depth study of breakthrough behavior was conducted to utilize activated carbon beads [25]. The activated carbons, zeolites, and molecular sieves were employed to explore the kinetics and equilibrium [26]. The effect of superficial velocity on the breakthrough response utilizing metal-organic framework (MOF) activated carbons, and crystalline pellets were investigated [27]. The beads of activated carbons were utilized to examine the adsorption equilibrium with a feed mixture of CO_2 and N_2 [28]. A MOF (UTSA-16, UTSA stands for University of Texas at San Antonio) was utilized for CO_2 separation, and the maximal adsorption capacity of 1.60×10^2 cm^3/cm^3 was reported [29]. The adsorption response of polyaspartamide was predicted using models based on kinetics, and it was concluded that adsorption is credited to external mass transfer [30]. Adsorption of CO_2 employing various adsorbents was examined, and the maximal capacity was reported for activated carbons [31]. The parametric study and breakthrough behavior with specific emphasis on the mass transfer zone (MTZ) by utilizing two grades of activated carbons employing a fixed bed column were carried out [32,33].

Numerous biomass materials have been used to synthesize activated carbon for the CO_2 adsorption study. Investigators have used macadamia shell biomass to prepare activated carbons using the microwave irradiation technique [34]. Additionally, the walnut shell has also been used to synthesize activated carbon and employed for manufacturing the cartridge [35]. Activated carbon fiber was prepared, and a capacity of 1.3×10^{-3} mol/g adsorbent was achieved [36]. The capacity of 9.09×10^{-3} mol/g was reported for synthesized activated adsorbent prepared by treating coal with potassium hydroxide (KOH) [37]. Activated carbons/N-enriched activated carbons were utilized for CO_2 separation and replicated the breakthrough curve satisfactorily [38]. A synthesized adsorbent of 13X and activated carbon was used for CO_2 separation and seen to have a capacity of 2.63 mmol/g [39].

The optimal incorporation of carbon nanotubes into the zeolites 13X was carried out, and the increased adsorption capacity was reported [40]. Microporous biochar adsorbent was employed to capture the adsorbate in a fixed bed for experimental and simulation study [41]. The amine adsorbents were synthesized using fly ash (FA), and the increased capacity of polyethylenimine/FA type- adsorbents was reported [42]. Biomass-based on palm shell-derived activated carbon was applied for preparing the activated carbon using chemical activation, and various metal oxides were employed for impregnation. The prolonged breakpoint time of 350 s with a capacity of 0.63 mmol CO_2/g AC for AC-PKS (palm kernel shell)/CeO_2 was reported [43]. Researchers have used walnut and almond shell to synthesize the activated carbons, and the internal structure was analyzed using scanning electron microscopy and Fourier-transform infrared spectroscopy [44]. Walnut shell-based biomass was converted into activated carbons, and KOH was reported as the prime favorable activation agent [45]. The chemical activation method [46] was applied to prepare activated carbons from walnut shell biomass, and the adsorption capability of the removal of benzene was explored using $ZnCl_2/H_3PO_4$. A similar fixed bed study of CO_2 adsorption using commercial activated carbon and modified activated carbon with ammonia was carried out [47] and maximal adsorption capacity of 0.67 mol/kg was reported at 30°C with a feed flow rate of 50 mL/min.

The novelty of the current work is to study the different aspects of the fixed bed CO_2 adsorption from a mixture of CO_2/N_2 using activated carbon and silica gel. The breakthrough response was analyzed as a function of temperature and feed rate. The adsorption capacity of the bed was assessed with temperature, feed rate, and CO_2 partial pressure. Also, the accuracy of the generated data was measured by repeatability and uncertainty analysis. The effectiveness of adsorbent was investigated in terms of length of mass transfer zone (L_{MTZ}), utilization factor (f), and temperature profiles inside the column.

2. Experiment setup

2.1. Chemicals

The activated carbon with a size range 0.4–0.8 cm was procured from Fluka™ analytical (Germany) and dried at 110°C in the drying oven before the experimental work. Silica gel (SG) with an average size range from 0.2 to 0.4 cm was procured from GCC Laboratory Reagent (UK) and dried at a temperature of 120°C before the experimental work. The selected adsorbents were used for experiments as such without any further treatment.

2.2. Setup diagram

The setup sketch of the fixed adsorption column (UOP15 – fixed-bed adsorption unit) with an effectual length

of 25 cm was used for the experiments, as depicted in Fig. 1. The feed flows to the adsorption unit from the bottom side according to the configuration of the column. The column was filled with AC and SG adsorbents up to the effective column length of 25 cm. This column is made up of stainless steel and jacketed to allow hot water to flow to attain the desired temperature using a water circulator. At the bottom of the column is a mesh of 50 mm diameter that retains glass beads of 2 mm diameter and a bed height of 5 mm to allow better distribution of the feed gas and to improve the temperature stability. Additionally, a triangular metal plate attached to the inside bottom of the column helps disperse the feed gas mixture. Flow controllers F_1, F_2, and F_3 measure and control the flow of N_2, CO_2, and CO_2 flow to the infrared (IR) sensor, respectively. It is recommended to work for a combined feed rate in the range of 0–5 L/min and maximal CO_2 concentration of 5% (vol.%) for the best results. The maximal operating pressure and temperature are fixed at 1.2 bars absolute and 343 K, respectively. There are 6 thermocouples positioned along the axial direction of the column.

2.3. Procedure

The gaseous mixture of a known composition consisting of CO_2 and N_2 enters the bottom of the column. The flow of CO_2 and N_2 are controlled by the flow controllers F_1 and F_2. The heating jacket is used to control the desired bed temperature and the proportional integral derivative controller is incorporated in the control console with the task of fixing the desired temperature. The column exit concentration is measured using an IR sensor. All the experiments are performed up to a maximal CO_2 concentration of 5% (vol.%). An IR detector used for CO_2 measurement at the bed outlet works well up to the maximal CO_2 concentration of 5% (vol.%), and the maximal CO_2 concentration of 5% is recommended for the best results. It was ensured every time that CO_2 was desorbed completely from the adsorbent bed before starting the next set of an experiment by monitoring the CO_2 desorption data, maintaining N_2 flow for a sufficiently long time displayed by the data logger.

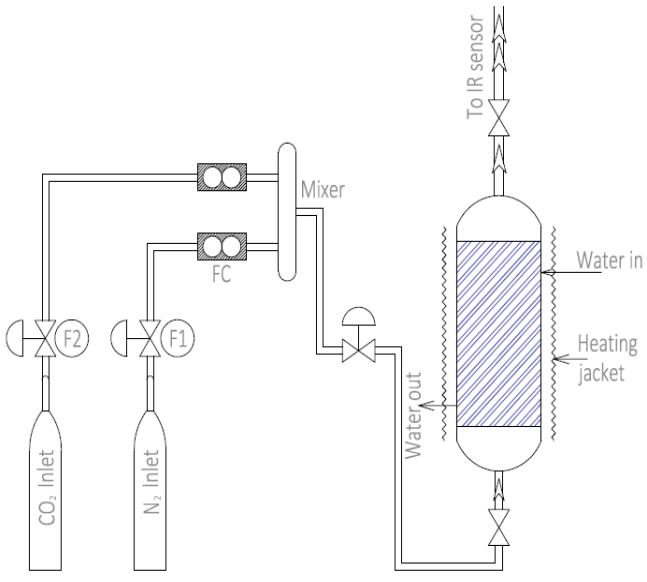

Fig. 1. Setup a diagram of the sorption unit.

3. Results and discussion

3.1. Adsorbent surface characterization

Surface area characterization of both the AC and SG was carried out using a surface analyzer (Quantachrome NOVAWin-NOVA Instruments, U.S.A.). The results obtained are summarized and depicted in Table 1. Single point surface areas of 858 and 590 m^2/g were exhibited by activated carbon and silica gel, respectively. The multipoint surface area of 862 m^2/g, which was nearly equal to the single-point surface area, was observed for the AC. The AC revealed a high pore volume of 0.425 cm^3/g compared to SG. The nearly same pore radii of 1.838 and 1.835 Å were reported for AC and SG, respectively.

The surface morphology of the AC and SG was analyzed by the Field Electron and Ion Company (FEI) scanning electron microscope (FEI-Quanta 250 high resolution, Czech Republic). The morphological images are shown in Fig. 2. It was observed that pore density was significantly higher for activated carbon compared to silica gel adsorbent and also the pores were uniformly distributed, as depicted in Figs. 2a and b.

3.2. Activated carbon

The reliance of sorption response (in terms of C/C_0) on time at different temperatures using the AC (wt. = 180 g) is depicted in Fig. 3. The experiments were performed at a feed rate of 6.67×10^{-5} m^3/s and a CO_2 concentration of 0.05 (vol. fraction). The sorption breakthrough time relies strongly on the sorption temperature. The maximal breakthrough time and saturation time of 870 and 1,050 s, respectively, were realized at a bed temperature of 298 K. The breakthrough time and saturation time declined to 725 and 915 s, respectively, upon increasing the temperature at 308 K. A reduced breakthrough time of 630 s was attained at a sorption temperature of 318 K. The sorption temperature of 328 K attributed to reduced breakthrough and saturation times of 530 and 675 s, respectively. The prolonged breakpoint time at decreased temperature signifies the enhanced sorption capacity.

On the other hand, the breakthrough curve is vastly steep and signifies the maximal utilization of the sorbent capacity. The utilization of maximal capacity at a breakpoint is desired for the economical separation for CO_2. The steepness of the response curve signifies the narrowness of MTZ. A narrow MTZ attributes to faster adsorption. In all the cases, minute differences in the width of MTZ were

Table 1
Brunauer–Emmett–Teller surface characterizations

Characteristics	Activated carbon	Silica gel
Single point surface area (m^2/g)	858	590
Multipoint surface area (m^2/g)	862	599
Micropore volume (cm^3/g)	0.425	0.273
Pore radius (Å)	1.838	1.835

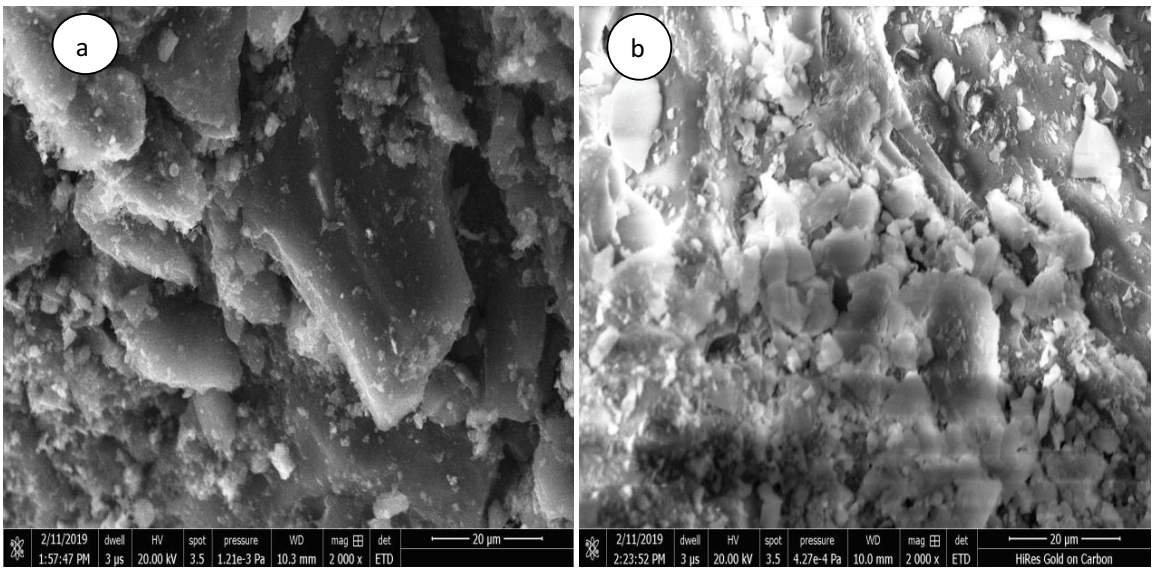

Fig. 2. Surface morphological images: (a) activated carbon and (b) silica gel at 2,000× magnification.

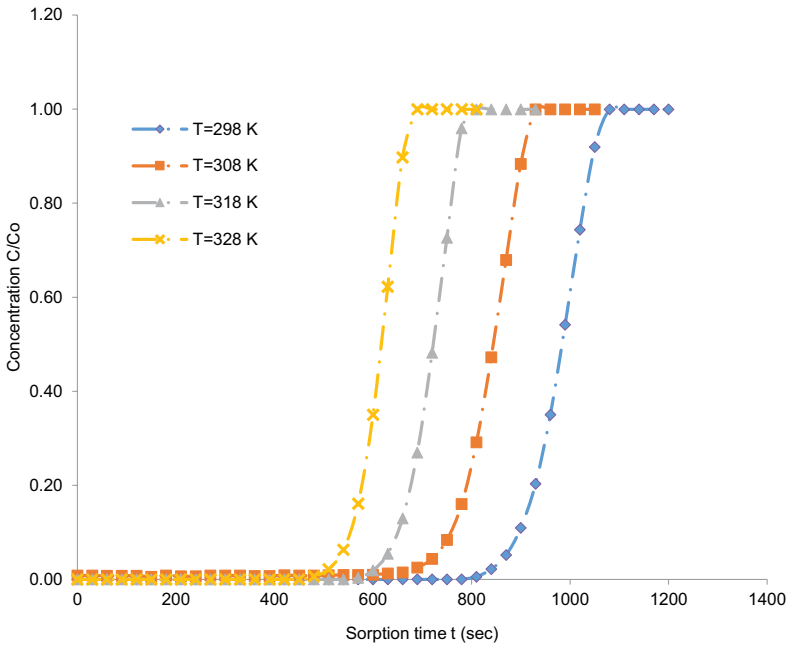

Fig. 3. Breakthrough response for activated carbon for AC ($F = 6.67 \times 10^{-5}$ m^3/s; $C_0 = 5\%$).

observed, which indicates almost the same utilization of bed capacity at the breakthrough point. The lowest layer of the bed is nearly saturated and mostly, the adsorption takes place over a comparatively narrow adsorption zone, wherein the concentration varies quickly. The breakthrough curve is vastly steep for a relatively narrow MTZ, and the majority of the bed capacity is used at the breakpoint. A narrow MTZ characterizing the competent use of the adsorbent leads to reduced costs of energy regeneration.

The sorption responses at various feed rates are depicted in Fig. 4. The feed rates of 5.00×10^{-5} m^3/s, 6.67×10^{-5} m^3/s, and 8.33×10^{-5} m^3/s were selected at a fixed temperature of 298 K. The breakthrough and saturation times vary significantly with feed rates. The prolonged breakpoint time of 1,145 s was attained at a feed rate of 5.00×10^{-5} m^3/s. The breakpoint time reduced from 1,145 to 975 s upon raising the feed rates from 5.00×10^{-5} m^3/s to 6.67×10^{-5} m^3/s. The minimal breakthrough and saturation times of 815 and 985 s, respectively, are exhibited by the AC at a feed rate of 8.33×10^{-5} m^3/s. The saturation and breakthrough periods reduced considerably with an increase in feed flow rate.

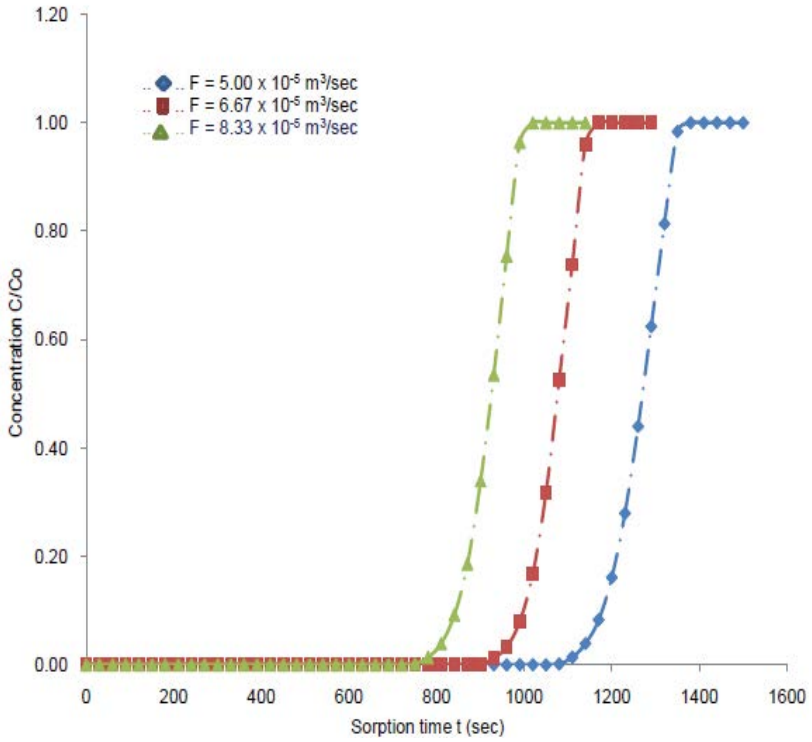

Fig. 4. Breakthrough sorption response at various feed rates for AC (T = 298 K; C_0 = 5%).

Also, the narrow MTZ exhibited by AC characterizes the suitability of carbon-based adsorbent for carbon dioxide separation from the CO_2/N_2 mixture. The steepness of the curve (*S*-shape) is very significant and highly desirable for economical adsorption. The MTZ moves up the column as feed mixture flow. After the breakpoint time is approached, the concentration C rises very quickly up to the end of the curve, where the bed is judged unproductive.

The sorption capacity is estimated by dynamic mass balance, which needs integration of the adsorption data. Utilizing the curve data, the time (t_s) of the total/stoichiometric capacity is normally tabulated by integrating the following equation [48]:

$$t_s = \int_0^\infty \left(1 - \frac{C}{C_0}\right) dt \tag{1}$$

where C is the CO_2 concentration at time t, and C_0 is the feed concentration of CO_2. Knowing t_s, the dynamic capacity q_t of the bed can be calculated as [49]:

$$q_t = \frac{F t_s C_0}{m_{ad}} \tag{2}$$

where F is the total feed molar flow rate, and m_{ad} is the mass of sorbent used in the bed. The portion of the column where the adsorbate is really adsorbed on the sorbent is known as the L_{MTZ}. The MTZ normally shifts from the inlet toward the exit during the sorption operation. This means that the sorbent adjacent to the inlet becomes saturated with the adsorbate first and then the sorption zone toward the end-side of the bed. A schematic depiction of the response curve and the shift of the MTZ are shown in Fig. 5. The L_{MTZ} was approximated assuming the constant pattern adsorption [50]:

$$L_{MTZ} = \frac{2L\left(t_s - t_b\right)}{t_s + t_b} \tag{3}$$

where L is the bed length, and t_b and t_s stand for breakthrough time and saturation time (exhaustion time), respectively. These are the times corresponding to the outlet concentrations of 5% and 95%, respectively. For the assumed symmetric breakthrough curve, the bed capacity utilization can be estimated using the utilization factor as:

$$f = 1 - \frac{0.5 L_{MTZ}}{L} \tag{4}$$

The characteristic parameters of sorption, that is, saturation time, breakthrough time, L_{MTZ}, and capacity utilization factor can be determined from the response curves (Figs. 3 and 4) for AC, as listed in Table 2. The breakthrough and saturation times decrease with increased sorption temperature, leading to longer MTZ. Also, these times reduced with feed flow rate, resulting in an increased L_{MTZ}. In common, the reduced temperature led to shorter MTZ owing to the increased nucleation of product species. The L_{MTZ} increases with an increase in temperature and flow rate. The maximal L_{MTZ} equal to 5.78 cm was realized at T = 328 K and feed rate of $F = 6.67 \times 10^{-5}$ m^3/s and reduced to 4.50 cm at a temperature of 298 K for AC. The utilization factor decreases with increased

sorption temperature and feed rate, and a maximal value of $f = 0.919$ was achieved at $T = 298$ K and $F = 5.00 \times 10^{-5}$ m^3/s.

The CO_2 sorption capacity variation with temperature is predicted in Fig. 6. The data were obtained at a feed rate of 6.67×10^{-5} m^3/s. The maximal adsorption capacity of 32.99 g CO_2/kg adsorbent was attained at a temperature of 298 K, but reduced to 26.00 g CO_2/kg adsorbent with an increased temperature of 308 K. The maximal sorption capacity of 22.44 g/kg adsorbent was obtained with a column temperature of 318 K. The sorption temperature of 328 K contributed to a CO_2 capacity of 11.22 g/kg adsorbent. It was found that the maximal selective capacity of the adsorbent for CO_2 strongly depended on the temperature and significantly reduced with an increase in the bed temperature. The reduced sorption temperature increases the selective capacity of CO_2 adsorption from the CO_2/N_2 feed mixture. The saturation adsorbent capacity varies significantly with bed temperature. The concentration of

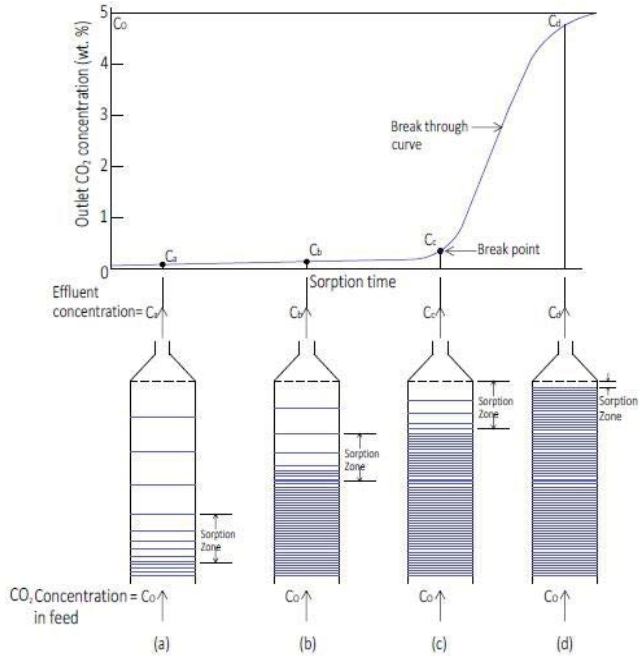

Fig. 5. Breakthrough and mass transfer zone.

Table 2
Effect of operating conditions on characteristics parameters for AC

T (K)	F, × 10^{-5} (m^3/s)	t_b (s)	t_s (s)	Length of mass transfer zone (L_{MTZ}) (cm)	Utilization factor (f)
298	6.67	870	1,050	4.50	0.906
308	6.67	725	915	5.56	0.884
318	6.67	630	778	5.05	0.895
328	6.67	530	675	5.78	0.879
298	5.00	1,145	1,345	3.86	0.919
298	8.33	815	988	4.60	0.904

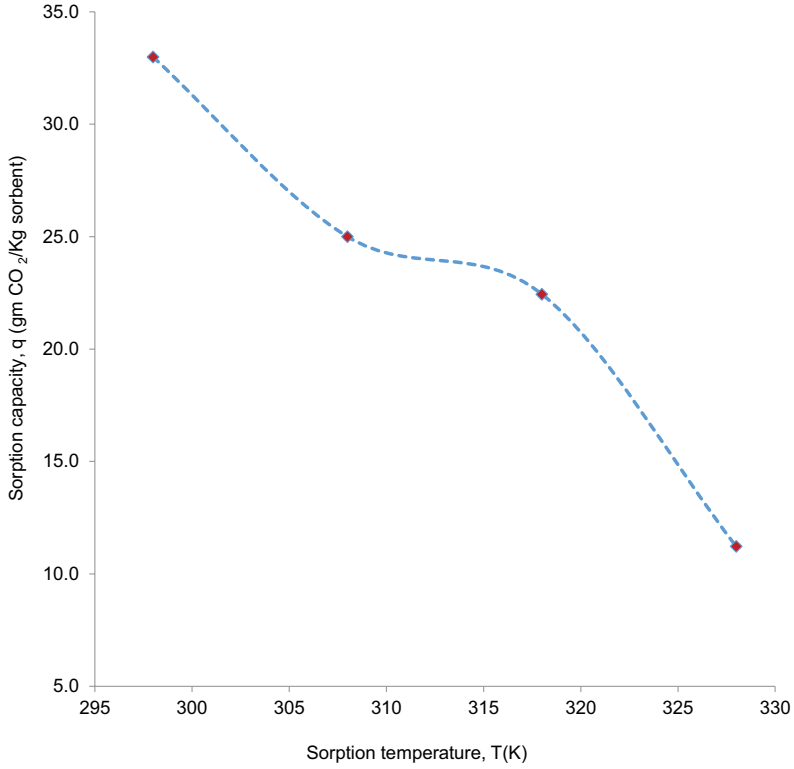

Fig. 6. Sorption capacity vs. temperature curve for AC ($F = 6.67 \times 10^{-5}$ m^3/s; $C_0 = 5\%$).

the adsorbed gas or the adsorption capacity lessens with an increase in the bed temperature at a given equilibrium pressure, as adsorption is an exothermic process.

The adsorption isotherms at a feed rate of 6.67×10^{-5} m^3/s utilizing AC are exhibited in Fig. 7. The impact of different temperatures on the sorption response was investigated at a fixed inlet CO_2 concentration of 5% (vol.%). The sorption capacity increases considerably with an increase in the pressure of the CO_2. At a bed temperature of 298 K, the maximal adsorption capacity of 32.99 g CO_2/g adsorbent was realized at an equilibrium partial pressure of 1.25×10^5 N/m^2. The capacity declined from 32.99 g CO_2/kg adsorbent to 12.20 g/kg adsorbent on reducing the CO_2 partial pressure from 1.25×10^5 N/m^2 to 0.50×10^5 N/m^2. At the same sorption temperature (T = 298 K), the adsorption capacity of 1.42 g CO_2/kg adsorbent was determined. For an adsorption isotherm produced at a bed temperature of 308 K, the minimal capacity of 1.09 g CO_2/kg adsorbent (P^* = 0.062×10^5 N/m^2) was exhibited by the adsorbent bed, and the capacity further enhanced to 20.14 g/kg adsorbent at a CO_2 pressure of 1.0×10^5 N/m^2. The sorption capacity of 22.441 g/kg adsorbent at a partial pressure of 1.25×10^5 N/m^2 was realized corresponding to a temperature of 318 K and capacity declined considerably to 10.34 g CO_2/kg adsorbent at a CO_2 pressure equal of 0.625×10^5 N/m^2. The minimal adsorption capacity of 0.941 g CO_2/g adsorbent was realized at a CO_2 partial pressure of 0.625×10^5 N/m^2. The maximal and minimal capacities of 11.22 g/kg adsorbent and 0.47 g/kg adsorbent were exhibited at equilibrium partial pressures of 1.25×10^5 N/m^2 and 0.063×10^5 N/m^2, respectively, by fixing the sorption temperature at 328 K.

At a constant partial pressure of 1.25×10^5 N/m^2, the capacity of 26.00 g CO_2/kg adsorbent was exhibited at a temperature of 308 K and declined to 22.44 g CO_2/kg adsorbent at a bed temperature of 318 K. Different gases are adsorbed to different extents under comparable conditions. It can be concluded that increasing the pressure of CO_2 will cause more of the adsorbable gas to be adsorbed, as the rising curve indicates. It may be concluded that the adsorption capacity increases remarkably with the partial pressure of CO_2.

The reliance of the feed rate on the capacity utilizing AC from a CO_2/N_2 mixture is depicted in Fig. 8. The bed temperature was fixed at 298 K, and the adsorbable gas concentration in the feed (CO_2) was adjusted at 5% (vol.%). The sorption capacity increases considerably with an increase in the feed (N_2 + CO_2) rate from 5.00×10^{-5} m^3/s to 8.33×10^{-5} m^3/s. The capacity of sorption of 32.36 g CO_2/kg sorbent was realized at a feed rate of 5.00×10^{-3} m^3/s and further enhanced to 36.39 g CO_2/kg sorbent upon raising the feed rate at 6.67×10^{-5} m^3/s. The maximal capacity of 39.14 g CO_2/kg sorbent was attained at a feed rate of 8.33×10^{-5} m^3/s. It was realized that as the increasing amount feed (fluid) is passed through the sorption column, the sorbent adsorbs an increasing amount of solute (CO_2) from the feed gas mixture yielding to increased sorption capacity. Therefore, it can be concluded that the sorption capacity of the sorbent enhances significantly with increasing feed rates. The higher feed rate favors the increased sorption capacity of the adsorbed gas from the feed mixture (N_2 + CO_2).

The adsorption isotherms obtained at T = 298 K with feed rates ranging from 5.00×10^{-5} m^3/s to 8.33×10^{-5} m^3/s are depicted in Fig. 9. The capacity enhances with a rise

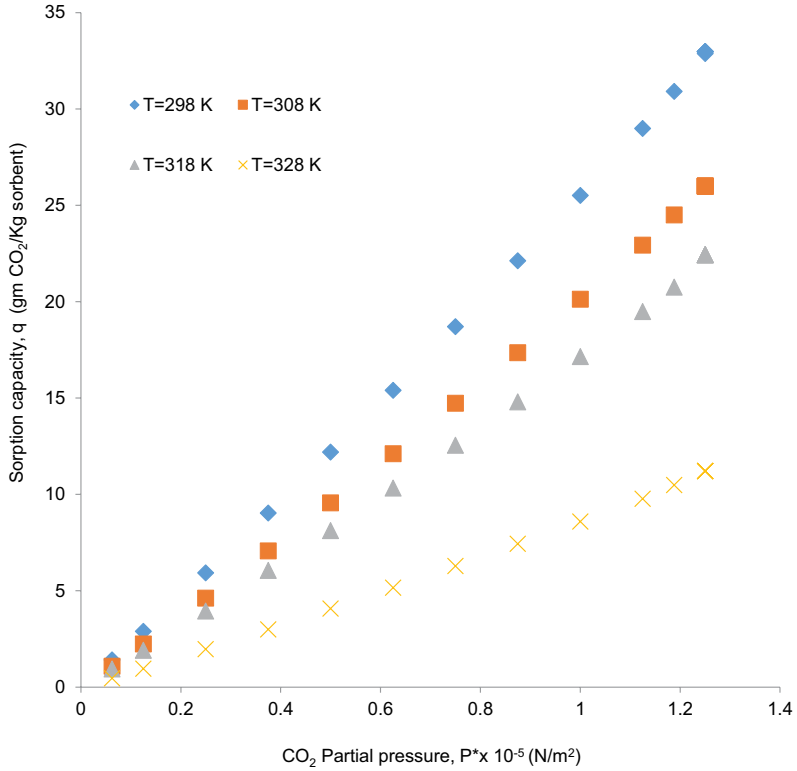

Fig. 7. Sorption capacity vs. partial pressure curves for AC (F = 6.67×10^{-5} m^3/s).

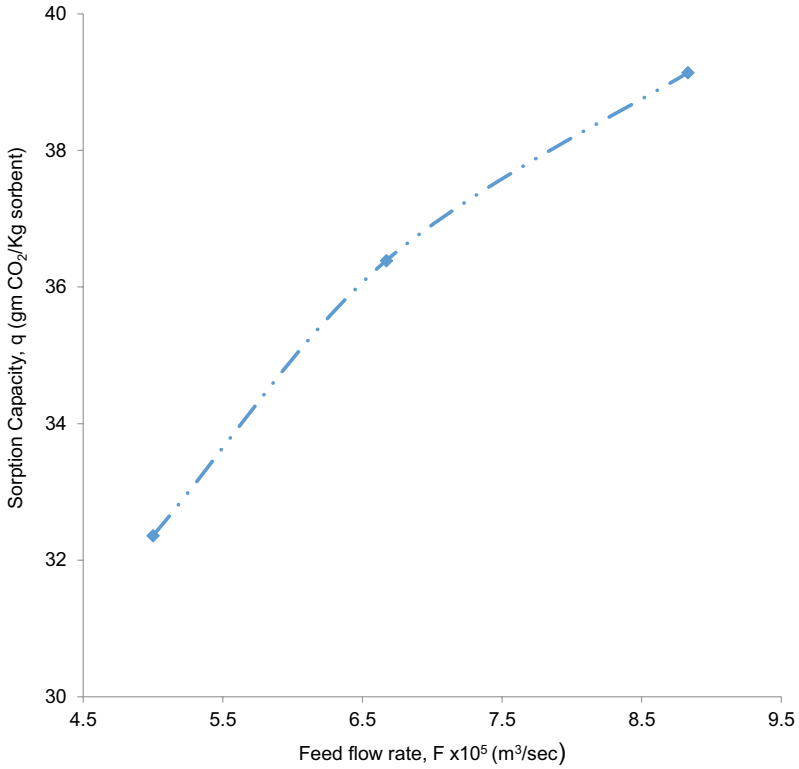

Fig. 8. Sorption capacity vs. feed flow rate for AC (T = 298 K).

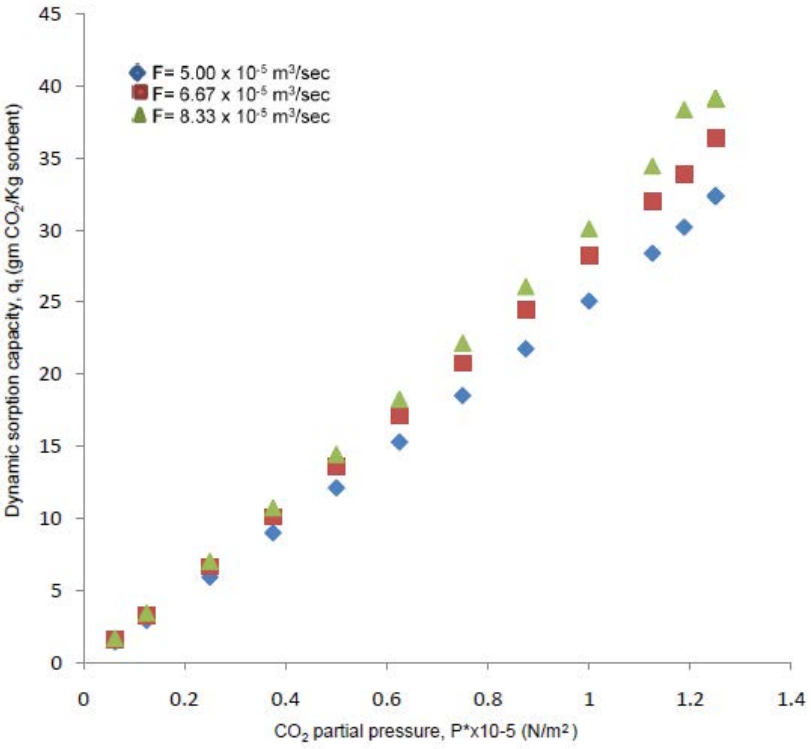

Fig. 9. Sorption capacity vs. CO_2 partial pressure curve (T = 298 K).

in the partial pressure of the adsorbable gas (CO_2). The minimal sorption capacity equal of 1.43 g CO_2/kg sorbent was obtained at a CO_2 pressure of 0.063×10^5 N/m^2 and the capacity increased to 25.07 g CO_2/kg adsorbent upon raising the CO_2 pressure to 1.0×10^5 N/m^2 at a feed rate of 5.00×10^{-5} m^3/s. The maximal capacity equal to 32.36 g CO_2/kg sorbent was exhibited at the CO_2 partial pressure of 1.25×10^5 N/m^2. The increased capacity of 28.23 g adsorbent/kg sorbent was determined at a CO_2 partial pressure equal to 1.0×10^5 N/m^2 on fixing the feed rate at 6.67×10^{-5} m^3/s. The maximal capacity increased to 36.39 g CO_2/kg sorbent at a partial pressure of 1.25×10^5 N/m^2 with a feed rate of 6.67×10^{-5} m^3/s. The minimal and maximal capacity of 1.68 g CO_2/kg sorbent and 39.14 g CO_2/kg sorbent with an increased feed rate to 8.33×10^{-5} m^3/s adsorbent were realized by controlling the partial pressures of 0.063×10^5 N/m^2 and 1.25×10^5 N/m^2, respectively. Generally, capacity improved remarkably with an increase in the feed flow of CO_2/N_2. The dependence of the capacity is more pronounced with adsorbable gas partial pressure compared to feed rates.

The temperature profiles of different temperature sensors (T1–T6) are depicted in Fig. 10. Temperature sensors T7 (308 K) represent hot water circulator temperature. The temperature rising above the set point during the initial sorption period attributes to the adsorption, which is exothermic in nature and accompanied by the liberation of heat. The temperature sensors are located at various positions in the column along the length. The temperatures T1 and T6 represent the top and bottom temperatures respectively, whereas the temperatures T2–T5 corresponds to the intermediate column temperature from the top to the bottom side. All the temperature sensors are insulated type-K thermocouples. The temperature sensors T1 and T2 are located at 42 and 83 mm from the top of the column, respectively. The sensors T3 and T4 are positioned at distances of 125 and 167 mm, respectively. Additionally, 208 and 250 mm are the positions of the bottom-side temperature sensors T5 and T6, respectively.

Due to the exothermic nature of adsorption, the mass transfer front is followed by a rise in temperature, which is supported by temperature profiles at different positions. Also, it was observed that like the concentration of CO_2, the heat generated due to adsorption led to a rise in the temperature inside the adsorption column.

The accuracy was judged using the repeatability measurement. Repeatability is measured by generating two sets of data at 298 K and a feed flow rate of 5.00×10^{-5} m^3/s. The closeness of the data depicted in Fig. 11 indicates the reliability of the data. *R*-squared (R^2) has been found to be equal to 0.9962, and its value near to 1 signifies a good correlation among the repeated measurements. The data obtained for CO_2 adsorption is of high quality and reliable. The closeness of the data obtained under the same operating conditions signifies the quality of the data obtained.

The uncertainty analysis (error analysis) was carried out for all the measurements. The error in the measurement of gaseous flow rate using mass flow controllers F_1, F_2, and F_3 as well as temperature measurement were determined. The uncertainty in the analysis of all the measurements is depicted in Table 3. The uncertainty in the measurement of temperature is estimated as ±0.15 K. The controllers F_1 (N_2 flow) and F_2 (CO_2 flow) contribute to uncertainty

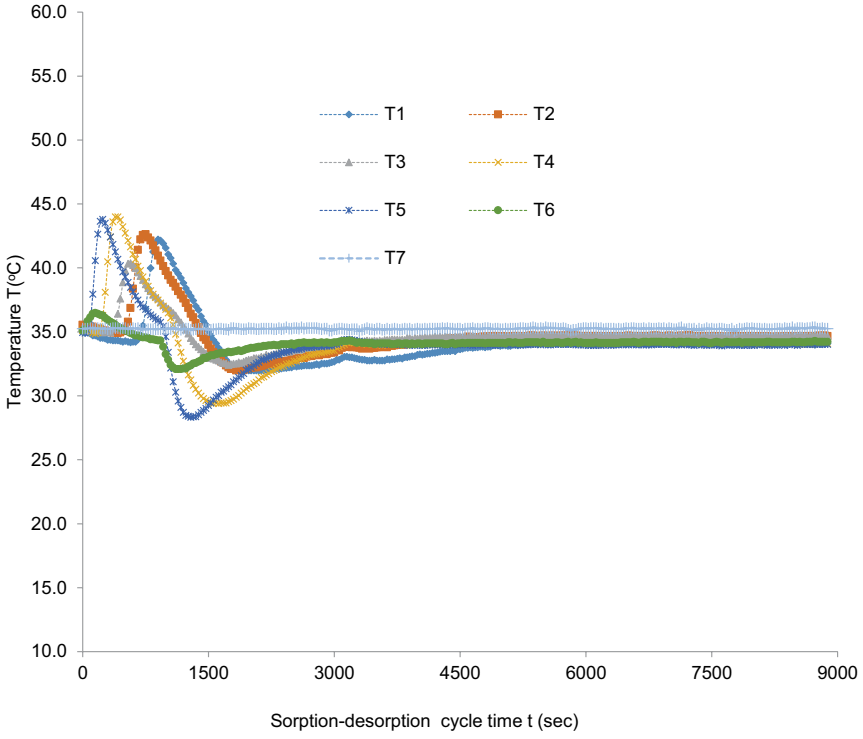

Fig. 10. Temperature profiles inside the sorption column employing AC ($F = 6.67 \times 10^{-5}$ m^3/s).

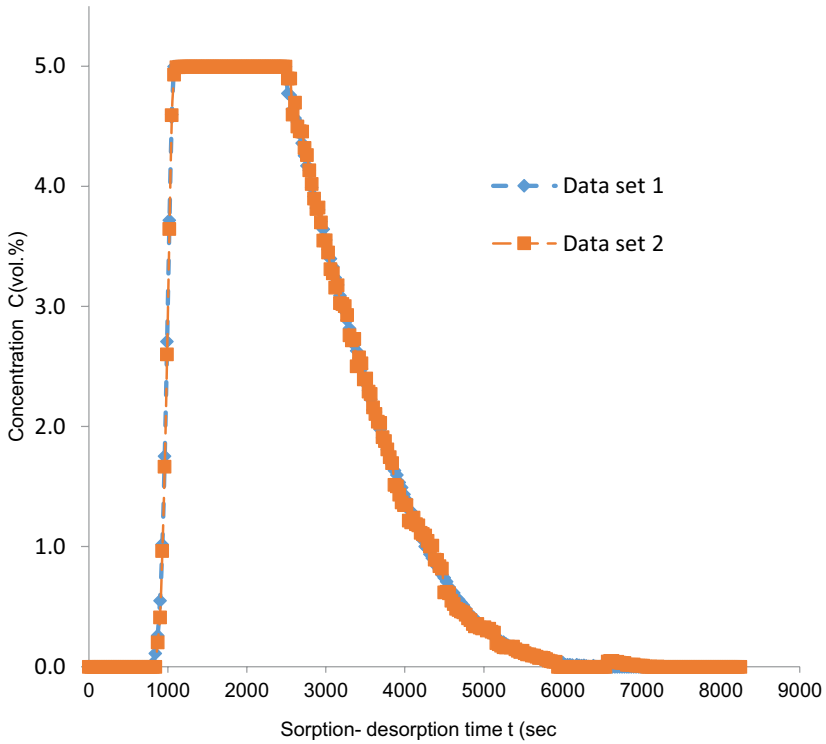

Fig. 11. Repeatability measurement for AC (T = 298 K; F = 5.00 × 10^{-5} m^3/s; C_0 = 5%).

Table 3
Uncertainty analysis of measured data

Variable (x)	Sensor type	Uncertainty (δx)
N_2 flow rate (m^3/s)	Mass flow meter (F_1)	±0.04
CO_2 flow rate (m^3/s)	Mass flow meter (F_2)	±0.02
IR feed flow (m^3/s)	Mass flow meter (F_3)	±0.01
Bed temperature (K)	Thermocouple type-K	±0.15

between ±0.04 and ±0.02 m^3/s, respectively. The uncertainty with the measurement of feed flow to the IR sensor using mass flow controller F_3 stands at ±0.01 m^3/s.

3.3. Silica gel

The sorption response curves generated at different temperatures using silica gel (wt. = 275 g) sorbent are depicted in Fig. 12. The feed rate was controlled at 6.67 × 10^{-5} m^3/s with the initial CO_2 concentration fixed at 0.05 (vol. fraction). The sorption periods alter significantly with the bed temperature. The breakthrough time and saturation time of 195 and 350 s, respectively, were estimated at a temperature of 298 K. The breakpoint time reduced to 152 s upon raising the temperature to 308 K with a saturation time of 290 s. The bed temperature of 318 K contributed to the decline in the breakpoint time and saturation time of 122 and 240 s, respectively. The breakpoint time and saturation time both retarded remarkably with an increase in the temperature. The prolonged breakthrough time and saturation time that characterize the capacity of adsorption were reported for AC compared to the SG type sorbent. Under the same conditions of sorption temperature, that is, 298 K and feed rate (6.67 × 10^{-5} m^3/s), the breakpoint periods between 870 and 195 s were exhibited for AC and SG, respectively. The breakpoint time reported for AC is almost more than 4 times that reported for SG at a fixed temperature (T = 298 K) and feed rate (F = 6.67 × 10^{-5} m^3/s). In the case of SG, the time required to reach the saturation condition of the bed from the breakthrough point is 155 s at a sorption temperature of 298 K compared to a lower value of 118 s at a temperature of 318 K.

The influence of the feed rates on the sorption response of CO_2 separation utilizing SG is exhibited in Fig. 13. The sorption response was analyzed at feed rates of 5.00 × 10^{-5} m^3/s, 6.67 × 10^{-5} m^3/s and 8.33 × 10^{-5} m^3/s controlling the temperature at 298 K. The prolonged breakpoint and saturation times of 250 and 425 s, respectively, are exhibited for SG adsorbent at a feed rate of 5.00 × 10^{-5} m^3/s. The breakpoint time declined to 195 s on increasing the feed rate to 6.67 × 10^{-5} m^3/s. The saturation time of 370 s was reported at a constant feed rate of 6.67 × 10^{-5} m^3/s. The breakthrough and saturation times of 180 and 340 s, respectively, were achieved at a maximal feed rate of 8.33 × 10^{-5} m^3/s.

The characteristic parameters of the CO_2 sorption determined from the breakthrough curves (Figs. 12 and 13) for SG are depicted in Table 4. In general, the reduced breakthrough and saturation time have been obtained for SG compared to AC. The breakthrough and saturation times reduce with an increase in temperature, resulting in longer MTZ. Also, these times reduce with an increase in the feed flow rate, resulting in an increase in the L_{MTZ}. In general, the L_{MTZ} increases with a rise in temperature and feed rate. The maximal value of L_{MTZ} = 15.65 cm was obtained at a

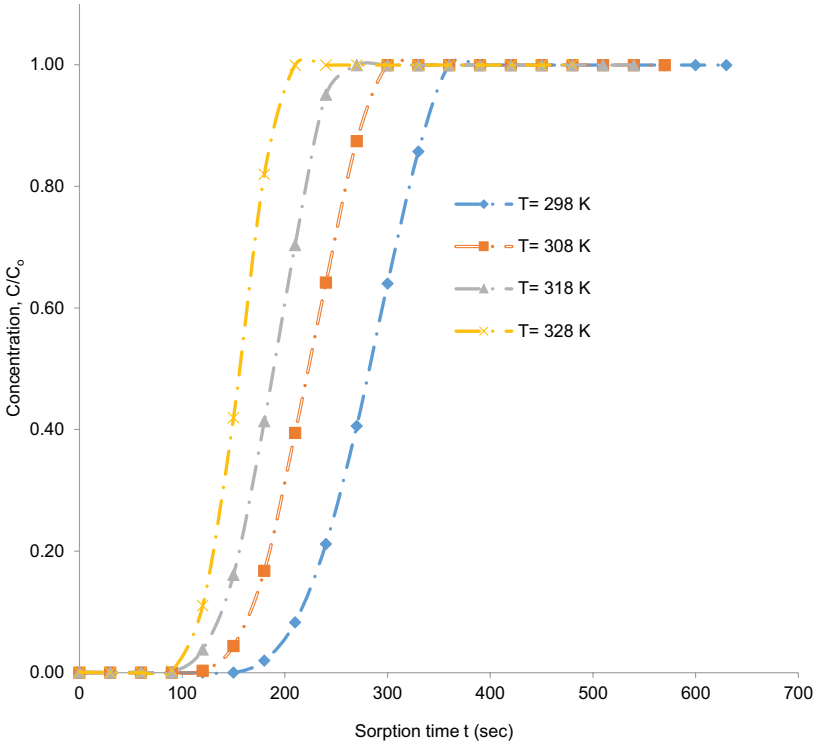

Fig. 12. Sorption response at different temperatures for SG (F = 6.67 × 10^{-3} m^3/s; C_0 = 5%).

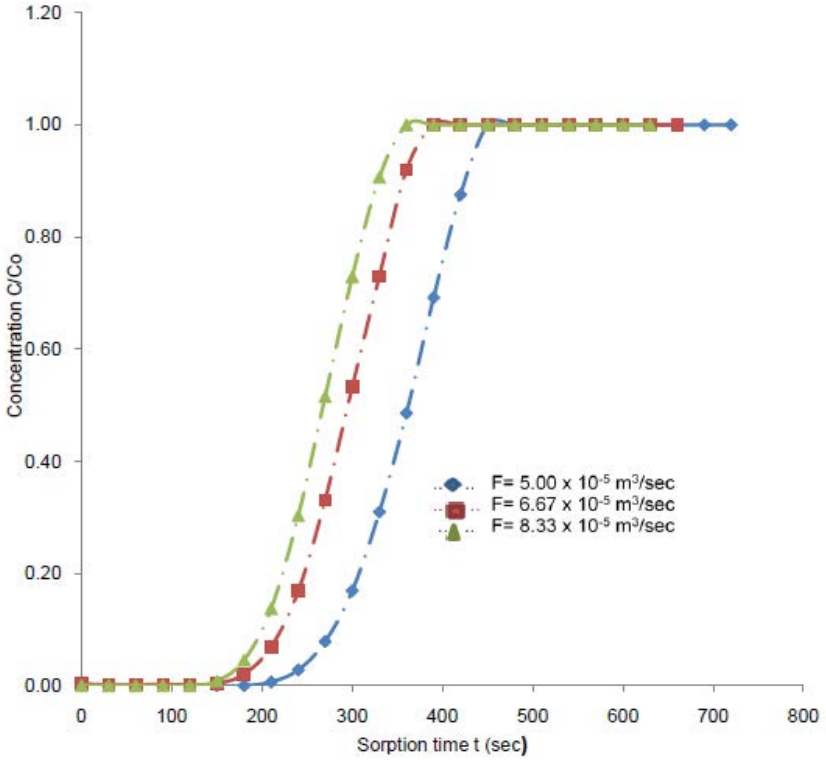

Fig. 13. Sorption response at different feed rates for SG (T = 298 K; C_0 = 5%).

Table 4
Effect of operating conditions on characteristics parameters for SG

T (K)	F, × 10^{-5} (m^3/s)	t_b (s)	t_s (s)	Length of mass transfer zone (L_{MTZ}) (cm)	Utilization factor (f)
298	6.67	195	350	13.65	0.706
308	6.67	152	290	14.99	0.688
318	6.67	122	240	15.65	0.674
328	6.67	105	206	15.59	0.675
298	5.00	250	425	12.44	0.740
298	8.33	180	340	14.77	0.692

temperature of 318 K and a feed flow rate of 6.67 × 10^{-5} m^3/s. The utilization factor decreases with an increase in sorption temperature and feeds flow rate. The maximal utilization factor f = 0.740 was determined at T = 298 K and F = 5.00 × 10^{-5} m^3/s for SG. The capacity utilization factor obtained for AC is significantly higher compared to that of SG under the same operating condition of temperature and feed rate. Also, the L_{MTZ} determined for AC is considerably small in comparison with L_{MTZ} of SG.

The dependence of sorption capacity on the temperature for SG is depicted in Fig. 14. The data were generated at a superficial velocity of 6.67 × 10^{-5} m^3/s. The capacity of sorption reduced considerably with an increased sorption temperature. The maximal sorption capacity of 6.35g CO_2/kg sorbent was achieved at a temperature of 298 K and it declined to 4.95g CO_2/kg sorbent on raising the temperature to 308 K. The bed temperature of 318 K contributed to a CO_2 capacity of 4.19 g CO_2/kg sorbent at similar operating conditions. The capacity further reduced to 3.30 g CO_2/kg adsorbent on raising the sorption temperature at 328 K. It was clearly demonstrated that the adsorption capacity of the adsorbable gas (CO_2) declined notably with the increase in the bed temperature (Fig. 14). The concentration of the adsorbed gas or adsorption capacity lessened with an increase in the temperature at a given equilibrium pressure. The capacity exhibited by the silica gel is considerably lower compared to that obtained for activated carbon at the same temperature.

The adsorption isotherms produced at sorption temperatures ranging from 298 to 328 K for SG are presented in Fig. 15. The sorption capacity increases considerably with

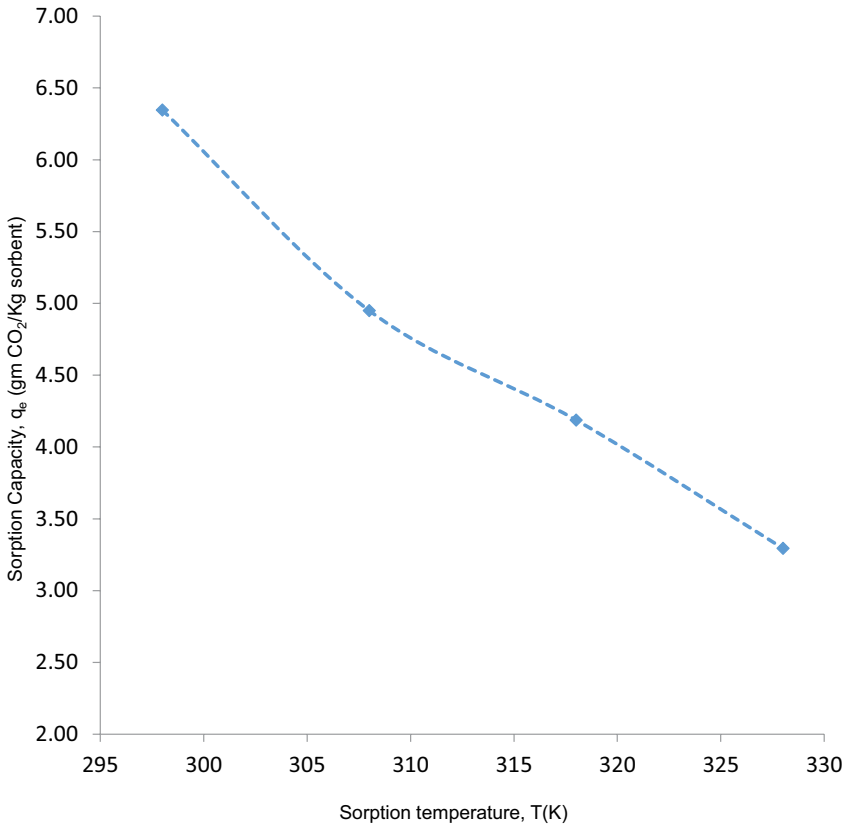

Fig. 14. Sorption capacity vs. temperature curve for SG (Q = 6.67 × 10^{-5} m^3/s; C_0 = 5%).

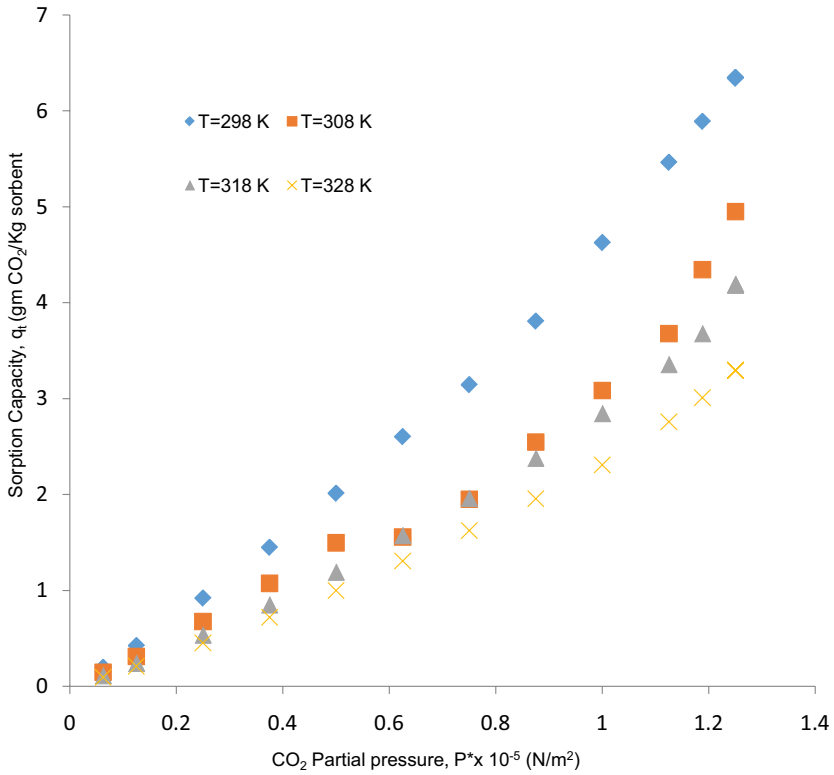

Fig. 15. Sorption capacity vs. partial pressure curves for SG (F = 6.67 × 10^{-5} m^3/s).

an increase in CO_2 pressure. The capacity of 4.63 g/kg sorbent was determined at a CO_2 pressure of 1.0 × 10^5 N/m^2 for isotherms generated at T = 298 K. At the same sorption temperature of T = 298 K, the minimal and maximal capacity of 0.20 g CO_2/kg sorbent and 6.35 g CO_2/kg sorbent was attained at CO_2 partial pressures of 0.063 × 10^5 N/m^2 and 1.250 × 10^5 N/m^2, respectively. At an increased sorption temperature of 308 K, the maximal capacity of 4.95 g CO_2/kg sorbent was attained at a fixed partial pressure of 1.25 × 10^5 N/m^2. Similar trends of capacity variation with CO_2 partial pressure have also been realized at an increased sorption temperature of 318 K, fixing the feed rate equal to 6.67 × 10^{-5} m^3/s. The capacity of adsorption further declines on raising the temperature to 328 K. The adsorption capacity of 1.0 g CO_2/kg sorbent was estimated at a CO_2 partial pressure of 0.5 × 10^5 N/m^2 and further increased to 2.76 g CO_2/kg sorbent on raising the partial pressure at 1.13 × 10^5 N/m^2. The maximal capacity of 3.3 g CO_2/kg sorbent was determined at a maximal partial pressure of 1.25 × 10^5 N/m^2.

The impact of the feed rate on the capacity of CO_2 utilizing the SG sorbent from a mixture of CO_2 + N_2 has been depicted in Fig. 16. The temperature was fixed at 298 K and the adsorbable gas concentration in feed was adjusted at 5% (vol.%). It is noticed that the capacity increases considerably with increased feed flow rate (N_2 + CO_2). The capacity of adsorption of 5.91 g CO_2/kg sorbent was realized at the feed flow rate of 5.00 × 10^{-5} m^3/s. It was further increased to 6.78 g CO_2/kg sorbent on raising the feed flow rate to 6.67 × 10^{-5} m^3/s. The maximal adsorption capacity equal to 7.64 g CO_2/kg sorbent was attained at a feed rate of 8.33 × 10^{-5} m^3/s. It was realized that as the increasing amount of feed (fluid) is passed through the adsorption column, the adsorbent adsorbs an increasing amount of solute (CO_2) from the feed gas mixture resulting in increased adsorption capacity. Therefore, it can be concluded that the adsorption capacity of the sorbent enhanced significantly with feed rate. The higher feed flow favors the increased adsorption capacity of the adsorbed gas from the feed mixture (N_2 + CO_2). It is suggested that higher feed flow is advantageous for achieving a higher adsorption capacity.

The adsorption isotherms obtained at T = 298 K for the feed rate ranging from 5.00 × 10^{-5} m^3/s to 8.33 × 10^{-5} m^3/s have been depicted in Fig. 17. The sorption capacity improves with raised CO_2 pressure. The minimal capacity equal to 0.188 g CO_2/kg sorbent was realized at a CO_2 pressure of 0.06 × 10^5 N/m^2 and the capacity increased to 1.49 g CO_2/kg sorbent on raising the pressure at 0.38 × 10^5 N/m^2 under the constant feed rate of 5.00 × 10^{-5} m^3/s. The maximal capacity equal to 5.91 g CO_2/kg sorbent was achieved at a CO_2 pressure of 1.25 × 10^5 N/m^2. The capacity increase of 4.85 g /kg sorbent was tabulated at a CO_2 partial pressure of 1.0 × 10^5 N/m^2 with an increased feed flow rate of 6.67 × 10^{-5} m^3/s. The maximal capacity improved to 6.78 g CO_2/kg sorbent at a partial pressure of 1.25 × 10^5 N/m^2 under a fixed feed rate of 6.67 × 10^{-5} m^3/s. The minimal and maximum capacity of 0.22 g CO_2/kg sorbent and 7.64 g CO_2/kg sorbent with an increased feed rate of 8.33 × 10^{-5}m^3/s was realized at partial pressures of 0.06 × 10^5 N/m^2 and 1.25 × 10^5 N/m^2, respectively. Generally, the sorption capacity of the sorbent improved remarkably with increased feed flow of the

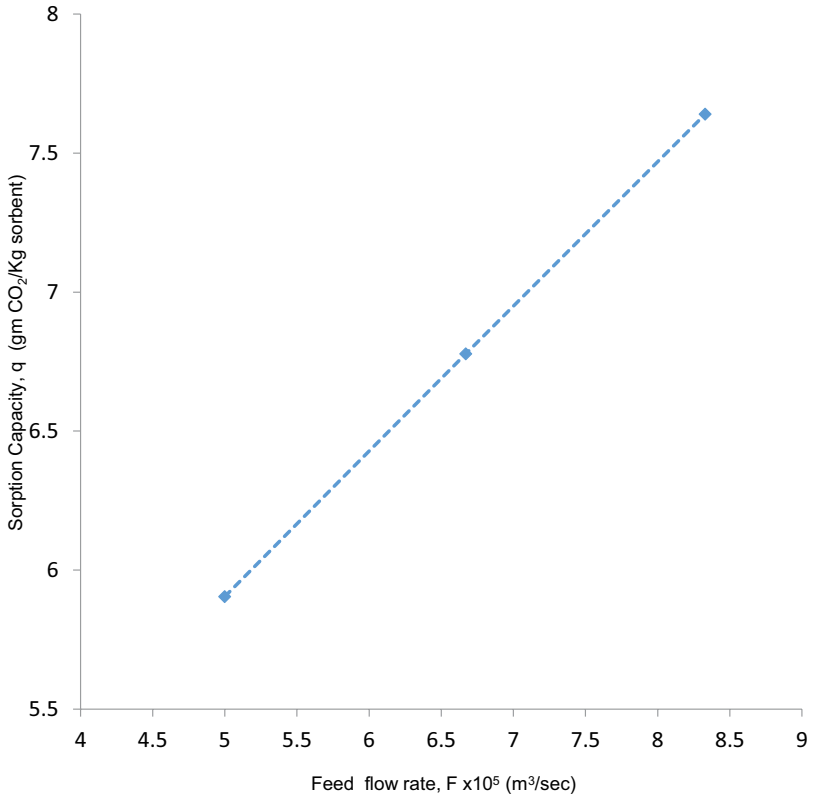

Fig. 16. Sorption capacity vs. feed flow rate for SG (T = 298 K).

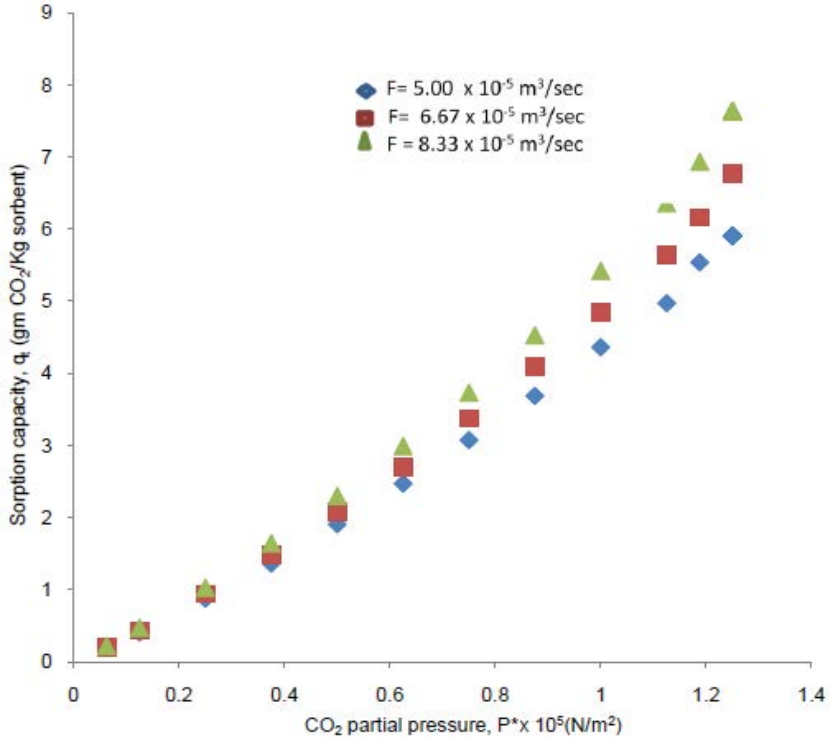

Fig. 17. Sorption capacity vs. partial pressure for SG (T = 298 K).

CO_2/N_2. The dependence of the sorption capacity is more pronounced with adsorbable gas partial pressures compared to feed rates.

4. Conclusion

The sorption breakthrough time relies strongly on the sorption temperature and reduces with an increase in temperature. The maximal breakthrough and saturation periods of 870 and 1050 s were exhibited for AC at a bed temperature of 298 K, respectively. The prolonged breakthrough and saturation times have been realized for AC compared to SG under constant operating conditions. The prolonged breakthrough time results in increased adsorption capacity. The breakthrough curves of AC are vastly steep signifying the maximal utilization of bed capacity at the breakpoint. A narrow MTZ characterizes the efficient use of the sorbent resulting in the reduction of costs of energy regeneration. The breakthrough and saturation times reduce significantly with an increase in the feed rate, respectively, and the prolonged breakpoint time of 1,145 s was attained at a feed rate of 5.00×10^{-5} m^3/s for AC. These times are considerably higher than the values obtained for SG. In general, the L_{MTZ} increases with raised temperature and feed flow rate, and the maximal L_{MTZ} equal to 5.78 cm was determined at $T = 328$ K and $F = 6.67 \times 10^{-5}$ m^3/s for AC. The utilization factor reduces with an increase in temperature and feed rate. The maximal utilization factors of 0.919 and 0.740 were determined at $T = 298$ K and $F = 5.00 \times 10^{-5}$ m^3/s for AC and SG, respectively, signifying the relevance of AC for CO_2 separation. The CO_2 capacity strongly depends on temperature and significantly reduces with an increase in bed temperature. The maximal capacities of 32.99 g CO_2/kg sorbent and 6.35 g CO_2/kg sorbent were determined at a temperature of 298 K for AC and SG, respectively. The capacity improves considerably with a rise in the pressure of CO_2, and AC exhibited higher sorption capacity compared to SG at a lower adsorption temperature of 298 K and flow rate of 6.67×10^{-5} m^3/s. The adsorption capacity increases considerably with increased feed rates ranging from 5.00×10^{-5} m^3/s to 8.33×10^{-3} m^3/s, and maximal capacity of 39.14 g CO_2/kg sorbent was determined for AC. AC may be used for economical separation of CO_2 from the N_2/CO_2 mixture owing to higher sorption capacity, good utilization factor, and smaller L_{MTZ}.

Acknowledgment

The research work was funded by the Deanship of Scientific Research (Project No. 310/1440), King Khalid University, Abha K.S.A.

References

[1] R.E. Hester, R.M. Harrison, Carbon Capture: Sequestration and Storage, RSC Publishing, Cambridge, 2010.
[2] L. Li, N. Zhao, W. Wei, Y. Sun, A review of research progress on CO_2 capture, storage, and utilization in Chinese academy of sciences, Fuel, 108 (2013) 112–130.
[3] N.A. Rashidi, S. Yusup, An overview of activated carbons utilization for the post-combustion carbon dioxide capture, J. CO_2 Util., 13 (2016) 1–16.
[4] IEA, CO_2 Capture at Power Stations and Other Point Sources: Zero Emission Technologies for Fossil Fuels, Organisation for Economic Co-operation and Development/International Energy Agency (OECD/IEA), Cedex, France, 2003.
[5] S.-Y. Lee, S.-J. Park, A review on solid adsorbents for carbon dioxide capture, J. Ind. Eng. Chem., 23 (2015) 1–11.
[6] R.T. Watson, Intergovernmental Panel on Climate Change, Climate Change 2001: Synthesis Report, Cambridge University Press, Cambridge, 2001.
[7] A. Alabadi, S. Razzaque, Y. Yang, S. Chen, B. Tan, Highly porous activated carbon materials from carbonized biomass with high CO_2 capturing capacity, Chem. Eng. J., 281 (2015) 606–612.
[8] J.D. Figueroa, T. Fout, S. Plasynski, H. McIlvried, R.D. Srivastava, Advances in CO_2 capture technology—the U.S. Department of Energy's Carbon Sequestration Program, Int. J. Greenhouse Gas Control, 2 (2008) 9–20.
[9] J. Gibbins, H. Chalmers, Carbon capture and storage, Energy Policy, 36 (2008) 4317–4322.
[10] E. Blomen, C. Hendriks, F. Neele, Capture technologies: improvements and promising developments, Energy Procedia, 1 (2009) 1505–1512.
[11] W.-J. Choi, J.-B. Seo, S.-Y. Jang, J.-H. Jung, K.-J. Oh, Removal characteristics of CO_2 using aqueous MEA/AMP solutions in the absorption and regeneration process, J. Environ. Sci., 21 (2009) 907–913.
[12] J. Gomes, S. Santos, J. Bordado, Choosing amine-based absorbents for CO_2 capture, Environ. Technol., 36 (2015) 19–25.
[13] M. Gupta, I. Coyle, K. Thambimuthu, CO2 Capture Technologies and Opportunities in Canada, Strawman Document for CO_2 Capture and Storage (CC&S) Technology Roadmap, CANMET Energy Technology Centre, Natural Resources Canada, Calgary, Alberta, Canada, 2003.
[14] A. Brunetti, F. Scura, G. Barbieri, E. Drioli, Membrane technologies for CO_2 separation, J. Membr. Sci., 359 (2010) 115–125.
[15] H.Q. Yang, Z.H. Xu, M.H. Fan, R. Gupta, R.B. Slimane, A.E. Bland, I. Wright, Progress in carbon dioxide separation and capture: a review, J. Environ. Sci., 20 (2008) 14–27.
[16] N. MacDowell, N. Florin, A. Buchard, J. Hallett, A. Galindo, G. Jackson, C.S. Adjiman, C.K. Williams, N. Shah, P. Fennell, An overview of CO_2 capture technologies, Energy Environ. Sci., 3 (2010) 1645–1669.
[17] S.M. Cohen, H.L. Chalmers, M.E. Webber, C.W. King, Comparing post-combustion CO_2 capture operation at retrofitted coal-fired power plants in the Texas and Great Britain electric grids, Environ. Res. Lett., 6 (2011) 024001.
[18] S. García, M.V. Gil, C.F. Martín, J.J. Pis, F. Rubiera, C. Pevida, Breakthrough adsorption study of a commercial activated carbon for pre-combustion CO_2 capture, Chem. Eng. J., 171 (2011) 549–556.
[19] J.M. Valverde, F. Pontiga, C. Soria-Hoyo, M.A.S. Quintanilla, H. Moreno, F.J. Duran, M.J. Espin, Improving the gas-solids contact efficiency in a fluidized bed of CO_2 adsorbent fine particles, Phys. Chem. Chem. Phys., 13 (2011) 14906–14909.
[20] J.-R. Li, Y.G. Ma, M.C. McCarthy, J. Sculley, J.M. Yu, H.-K. Jeong, P.B. Balbuena, H.-C. Zhou, Carbon dioxide capture-related gas adsorption and separation in metal-organic frameworks, Coord. Chem. Rev., 255 (2011) 1791–1823.
[21] M. Alonso, N. Rodríguez, B. González, G. Grasa, R. Murillo, J.C. Abanades, Carbon dioxide capture from combustion flue gases with a calcium oxide chemical loop. Experimental results and process development, Int. J. Greenhouse Gas Control, 4 (2010) 167–173.
[22] F. Raganati, P. Ammendola, R. Chirone, CO_2 capture by adsorption on fine activated carbons in a sound assisted fluidized bed, Chem. Eng. Trans., 43 (2015) 1033–1038.
[23] J.C. Abanades, E.J. Anthony, D.Y. Lu, C. Salvador, D. Alvarez, Capture of CO_2 from combustion gases in a fluidized bed of CaO, AlChE J., 50 (2004) 1614–1622.
[24] J.M. Valverde, F.J. Duran, F. Pontiga, H. Moreno, CO_2 capture enhancement in a fluidized bed of a modified Geldart C powder, Powder Technol., 224 (2012) 247–252.

[25] C.Z. Shen, J. Yu, P. Li, C.A. Grande, A.E. Rodrigues, Capture of CO_2 from flue gas by vacuum pressure swing adsorption using activated carbon beads, Adsorption, 17 (2011) 179–188.
[26] A.I. Sarker, A. Aroonwilas, A. Veawab, Equilibrium and kinetic behavior of CO_2 adsorption onto zeolites, carbon molecular sieve and activated carbons, Energy Procedia, 114 (2017) 2450–2459.
[27] N. Al-Janabi, R. Vakili, P. Kalumpasut, P. Gorgojo, F.R. Siperstein, X.L. Fan, P. McCloskey, Velocity variation effect in fixed bed columns: a case study of CO_2 capture using porous solid adsorbents, AlChE J., 64 (2018) 2189–2197.
[28] C.Z. Shen, C.A. Grande, P. Li, J. Yu, A.E. Rodrigues, Adsorption equilibria and kinetics of CO_2 and N_2 on activated carbon beads, Ind. Eng. Chem. Res., 160 (2010) 398–407.
[29] S.C. Xiang, Y.B. He, Z.J. Zhang, H. Wu, W. Zhou, R. Krishna, B.L. Chen, Microporous metal-organic framework with potential for carbon dioxide capture at ambient conditions, Nat. Commun., 3 (2012) 954.
[30] K.O. Yoro, M. Singo, J.L. Mulopo, M.O. Daramola, Modeling and experimental study of the CO_2 adsorption behavior of polyaspartamide as an adsorbent during post-combustion CO_2 capture, Energy Procedia, 114 (2017) 1643–1664.
[31] C.Y. Lu, H.L. Bai, B. Wu, F.S. Su, J.F. Hwang, Comparative study of CO_2 capture by carbon nanotubes, activated carbons, and zeolites, Energy Fuels, 22 (2008) 3050–3056.
[32] M.K. Al Mesfer, M. Danish, Y.M. Fahmy, M.M. Rashid, Post-combustion CO_2 capture with activated carbons using fixed bed adsorption, Heat Mass Transfer, 54 (2018) 2715–2724.
[33] M.K. Al Mesfer, M. Danish, Breakthrough adsorption study of activated carbons for CO_2 separation from flue gas, J. Environ. Chem. Eng., 6 (2018) 4514–4524.
[34] N. Dejang, O. Somprasit, S. Chindaruksa, A preparation of activated carbon from macadamia shell by microwave irradiation activation, 2015 International Conference on Alternative Energy in Developing Countries and Emerging Economies, Energy Procedia, 79 (2015) 727–732.
[35] M. Jahangiri, S.J. Shahtaheri, J. Adl, A. Rashidi, H. Kakooei, A.R. Forushani, G. Nasiri, A. Ghorbanali, M.R. Ganjali, Preparation of activated carbon from walnut shell and its utilization for manufacturing organic-vapor respirator cartridge, Fresenius Environ. Bull., 21 (2012) 1508–1514.
[36] E.M. Calvo-Muñoz, F.J. García-Mateos, J.M. Rosas, J. Rodríguez-Mirasol, T. Cordero, Biomass waste carbon materials as adsorbents for CO_2 capture under post-combustion conditions, Front. Mater., 3 (2016) 23.
[37] A. Toprak, T. Kopac, Carbon dioxide adsorption using high surface area activated carbons from local coals modified by KOH, NaOH and $ZnCl_2$ agents, Int. J. Chem. Reactor Eng., 15 (2017) 0042, doi: https://doi.org/10.1515/ijcre-2016-0042.
[38] T.L.P. Dantas, S.M. Amorim, F.M.T. Luna, I.J. Silva Jr., D.C.S. de Azevedo, A.E. Rodrigues, R.F.P.M. Moreira, Adsorption of carbon dioxide onto activated carbon and nitrogen-enriched activated carbon: surface changes, equilibrium, and modeling of fixed-bed adsorption, Sep. Sci. Technol., 45 (2009) 73–84.
[39] M.J. Regufe, A.F.P. Ferreira, J.M. Loureiro, Y.X. Shi, A. Rodrigues, A.M. Ribeiro, New hybrid composite honeycomb monolith with 13X zeolite and activated carbon for CO_2 capture, Adsorption, 24 (2018) 249–265.
[40] N.A.A. Qasem, R. Ben-Mansour, H.A. Habib, Enhancement of adsorption carbon capture capacity of 13X with optimal incorporation of carbon nanotubes, Int. J. Energy Environ. Eng., 8 (2017) 219–230.
[41] M.G. Plaza, I. Durán, N. Querejeta, F. Rubiera, C. Pevida, Experimental and simulation study of adsorption in postcombustion conditions using a microporous biochar. 1. CO_2 and N_2 adsorption, Ind. Eng. Chem. Res., 55 (2016) 3097–3112.
[42] Z.H. Zhang, B.D. Wang, Q. Sun, Fly ash-derived solid amine sorbents for CO_2 capture from flue gas, Energy Procedia, 63 (2014) 2367–2373.
[43] A.R. Hidayu, N. Muda, Impregnated palm kernel shell activated carbon for CO_2 adsorption by pressure swing adsorption, Indian J. Sci. Technol., 10 (2017) 1–6.
[44] P. Patil, S. Singh, Y.M. Kumar, Preparation and study of properties of activated carbon produced from agricultural and industrial waste shells, Res. J. Chem. Sci., 3 (2013) 12–15.
[45] H.Y. Xia, S. Cheng, L.B. Zhang, J.H. Peng, Utilization of walnut shell as a feedstock for preparing high surface area activated carbon by microwave induced activation: effect of activation agents, Green Process. Synth., 5 (2016) 7–14.
[46] M. Mataji, B. Khoshandam, Benzene adsorption on activated carbon from walnut shell, Chem. Eng. Commun., 201 (2014) 1294–1313.
[47] M.S. Shafeeyan, W.M.A.W. Daud, A. Shamiri, N. Aghamohammadi, Modeling of carbon dioxide adsorption onto ammonia-modified activated carbon: kinetic analysis and breakthrough behavior, Energy Fuels, 29 (2015) 6565–6577.
[48] E.R. Monazam, J. Spenik, L.J. Shadle, Fluid bed adsorption of carbon dioxide on immobilized polyethylenimine (PEI): kinetic analysis and breakthrough behaviour, Chem. Eng. J., 223 (2013) 795–805.
[49] R. Serna-Guerrero, A. Sayari, Modeling adsorption of CO_2 on amine-functionalized mesoporous silica. 2: kinetics and breakthrough curve, Chem. Eng. J., 161 (2010) 182–190.
[50] A.A. Pota, A.P. Mathews, Effects of particle stratification on fixed bed absorber performance, J. Environ. Eng., 125 (1999) 705–711.